



# Multilayer thermal control for high-altitude vertical imaging aerial cameras

YANWEI LI,<sup>1</sup> GUOQIN YUAN,<sup>2</sup> XINWANG XIE,<sup>1</sup> LEIGANG DONG,<sup>1</sup> AND LONGHAI YIN<sup>1,\*</sup>

<sup>1</sup>Ji Hua Laboratory, Foshan, Guangdong 528000, China

<sup>2</sup>Changchun Institute of Optics and Fine Mechanics and Physics, Chinese Academy of Sciences, Changchun, Jilin 130033, China

\*Corresponding author: ylh761208@163.com

Received 6 April 2022; revised 12 May 2022; accepted 14 May 2022; posted 18 May 2022; published 8 June 2022

Aerial cameras play an important role in obtaining ground information. However, the complex and changeable aviation environment limits its application. Thermal control is vital in improving the environmental adaptability of the camera to obtain high-quality images. Conventional thermal control of aerial cameras is to directly implement active thermal control on the optical system, which is a single layer thermal control method. Such a method cannot isolate the optical system from the external environment. It results in a sharp increase in thermal control power consumption and in temperature gradient, which increases the difficulty of thermal control. Here, we propose a multilayer system-level thermal control approach by partitioning the aerial camera into two parts, i.e., the imaging system and the outline cabin. Two parts are connected by materials with poor thermal conductivity, and an air insulation interlayer is formed in between. Theoretical analysis is carried out to model the internal and external thermal environment of the aerial camera in a complex high-altitude environment. We study passive thermal control of the thermal insulation layer of the outline cabin, the optical window, the imaging optics, the CCD device, and the phase change material, and active thermal control of the thermal convection and heating film. Numerical modeling on the multilayer thermal control of the system is carried out and verified by the thermal equilibrium test and actual field flight test. The total power consumption of the thermal control system is 270 W. High-quality images are obtained when the temperature gradient of the optical lens is less than 5°C and the temperature of the CCD is lower than 30°C. Our technology is simple, accurate, low cost, and easy to implement compared to the conventional thermal control method. It effectively lowers the power consumption and reduces the difficulty of thermal control. © 2022

Optica Publishing Group

<https://doi.org/10.1364/AO.460335>

## 1. INTRODUCTION

Aerial cameras with high resolution, real-time performance, and a wide coverage area have been widely used in aerial remote sensing, aerial surveying and mapping, aerial rescue, and other fields [1–4]. Obtaining high-resolution and high-quality images is the ultimate goal of aerial cameras. In high-altitude aerial photography, temperature is a key factor affecting the image quality of the camera. The impact of temperature variation mainly has three aspects. First, it changes the size and optical performance of the optical elements. The change in the refractive index of the glass material causes the optical system to defocus and produces additional aberrations, which leads to deterioration of image quality. Second, it lowers the performance of CCD and reduces the imaging quality of the system. Lastly, it may produce frost and fog on the optical window, resulting in imaging failure. Therefore, thermal control technology is critical to stabilize the temperature of the camera's optical system and eliminate the impact of the temperature gradient of the optical system on the image quality of the camera.

Thermal control technology of space cameras has been well established [5–8]. So far, there are limited studies on thermal control of aerial cameras, especially system-level thermal control. Liu *et al.* [9] proposed an active thermal control method to improve the imaging quality of aerial photoelectric platforms. Liu *et al.* [10] focused on analyzing the different effects of temperature changes on the imaging resolution of long focal length aerial cameras, and advised the improvement, making it difficult to further improve the image resolution. Fan *et al.* [11] used passive control methods such as thermal insulation to make the aerial camera optical system exceed the thermal time constant and reduce the sensitivity of the optical system to the external thermal environment. Compared with the thermal control technology of space cameras, the thermal control technology of aerial cameras has similarities in terms of thermal control methods, thermal control strategies, and thermal simulation analysis methods. However, the thermal control technology of aerial cameras also has its own characteristics: first, aviation cameras experience a rapid temperature change when lifted from the ground, which will lead to a greater temperature impact on

the optical window and optical system. Second, aerial cameras stay in the troposphere or stratosphere of the atmosphere after level flight, which is a non-vacuum environment. It is necessary to consider factors such as convection heat transfer and aerodynamic heat due to the complicated environment. Third, the flight time of the carrier is limited, and the thermal control cycle is relatively short. Fourth, despite the fact that the carrier can provide kilowatt-level thermal control power consumption, there is a large temperature gradient due to the difference in thermal conductivity of actual components, which increases the difficulty of thermal control.

So far, conventional thermal control method of aerial cameras is to directly implement active or passive thermal control on the optical system, using conduction, convection, radiation, and other methods to control the temperature level and temperature gradient of important optical components in the optical system to meet the design requirements, so as to obtain high-quality imaging images. Liu *et al.* [12] designed a thermal control for the main optical system of a long focal length aerial camera with an external dimension of  $1.36 \text{ m} \times 0.6 \text{ m} \times 0.6 \text{ m}$ . Conduction, convection, and radiation heating methods are applied to achieve both axial and radial temperature differences of the R-C main optical system less than  $5^\circ\text{C}$ . Since conduction heat exchange between the main optical system and the external environment are not effectively isolated, the thermal control power consumption is very high, about 800 W. The system implementation is also complicated. Cheng *et al.* [13] proposed a thermal control design for an aeronautical optoelectronic platform with external dimensions of 0.58 m wide and 0.78 m high. Combining active and passive thermal control technology, they control the temperature gradient of the primary and secondary mirrors in the optical system (R-C system) to be no greater than  $5^\circ\text{C}$ . Similarly, conduction heat exchange exists between the primary and secondary mirror components and the main frame of the photoelectric platform. The thermal control power consumption is as high as  $\sim 370 \text{ W}$ . Besides, thermal control design does not include the optical window and CCD. Within the scope of the literature we can find, the thermal control design of both the aviation optoelectronic platforms and the long-focus aerial cameras is the single layer thermal control method. It is not able to effectively achieve thermal isolation of the optical system from the external environment, resulting in higher thermal control power consumption and higher cost.

Based on detailed analysis of the internal and external thermal environment of the high-altitude vertical imaging aerial cameras and the principle of heat transfer, we propose a generalized multilayer system-level thermal control method for aerial cameras, especially for those exposed to the external environment directly at work. Multilayer thermal control is realized by separating the aerial camera system into two parts, i.e., the imaging system and the outline cabin. A rubber damper with poor thermal conductivity connects the two parts, which suppress the vibration from the carrier platform and isolate the heat. For the first layer thermal control, a thermal insulation layer is attached to the inner surface of the outline cabin for passive thermal insulation, and an active thermal control of the thermal convection is applied to the optical window. For the second layer thermal control, an air insulation layer with low thermal conductivity is formed between the outline cabin and the imaging system.

For the third layer thermal control, a thermal insulation layer is attached to the outer surface of the imaging system, combined with optical element heating film thermal control and CCD phase change thermal control. Numerical simulation on the whole system is carried out to simulate the transient thermal response and thermo-optical experiment at high altitude, and a low-temperature and low-pressure environment is carried out to verify the effectiveness of the multilayer thermal control method. High-quality images are obtained in the actual flight test. The method mentioned above demonstrates effective thermal insulation on aerial cameras, reduces difficulties of system thermal control, and lowers the power consumption and implementation cost of active thermal control of the whole system.

The rest of the paper is organized as follows: Section 2 discusses the modeling and analysis of the internal and external thermal environment, Section 3 covers the multilayer thermal control design, Section 4 provides the thermal simulation results and data analysis, Section 5 shows thermal equilibrium test and actual flight results, and Section 6 features conclusions and highlights.

## 2. THERMAL ENVIRONMENT ANALYSIS

The high-altitude vertical imaging aerial camera uses a refraction optical system in the visible spectral range, as shown in Fig. 1(a). Three mirrors are used to deflect the light path and reduce the axial length. The scanning mirror is for vertical imaging, which expands the coverage area and compensates for image shift.

The external dimensions of the camera are  $1000 \text{ mm} \times 450 \text{ mm} \times 580 \text{ mm}$ , and the weight is 200 kg. According to the proposed multilayer thermal control method, the camera is designed in two parts—the outline cabin and the imaging system—and the two are connected by a rubber vibration damper, as shown in Fig. 1(b). The imaging system includes the scan head assembly, front lens group, focusing lens group, rear lens group, electric control box assembly, CCD assembly,

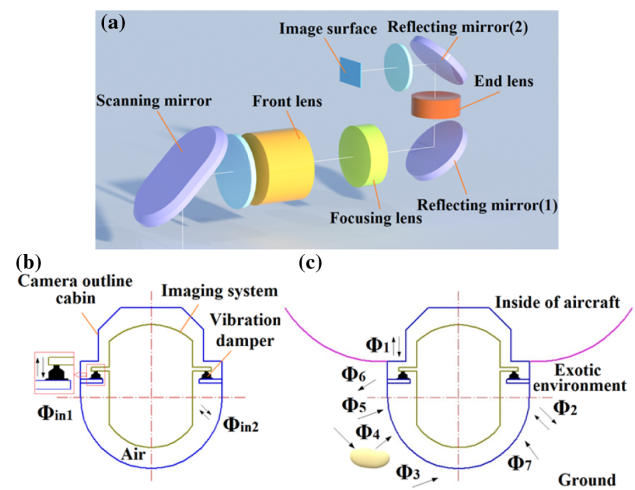


**Fig. 1.** (a) Schematics of the optical system of a high-altitude vertical imaging aerial camera, (b) cross-section schematics of the internal structure connection and internal heat exchange diagram of the aerial camera, and (c) schematic diagram of camera installation and external heat exchange.

focusing assembly, and shutter assembly. The entire imaging system is mounted on four vibration dampers installed in the outline cabin. The vibration damper is made of rubber material with poor thermal conductivity, so that the imaging system is isolated from thermal transfer from the external environment. The outline cabin is made from aluminum alloy including optical windows, storage, power box, etc. It retains conformity with the flight carrier and is relatively sealed, providing mechanical and optical interfaces for the imaging system.

The thermal environment of aerial cameras includes internal and external thermal environments. The internal thermal environment refers to the initial temperature of the camera and the internal heat source. The external thermal environment mainly refers to the atmospheric environment (altitude, temperature, density, pressure) during flight and flight speed.

### A. Internal Thermal Environment

As shown in Fig. 1(b), the heat exchange between the imaging system and the outline cabin is mainly conduction heat exchange  $\Phi_{in1}$  and radiation heat exchange  $\Phi_{in2}$ . Because the exterior outline cabin is sealed, the convective heat transfer between the imaging system and the outline cabin is negligible. The formula of conduction heat transfer is

$$\Phi = \frac{\Delta T}{R}, \tag{1}$$

where  $R$  is the thermal resistance, including conduction thermal resistance  $R_1$  and contact thermal resistance  $R_2$ ;  $\Delta T$  is the temperature difference between the two [14,15]. The conduction thermal resistance  $R_1$  is the resistance of the heat conduction within the part

$$R_1 = \frac{\delta}{\lambda A}, \tag{2}$$

where  $\lambda$  is the thermal conductivity of the material,  $A$  is the contact surface area,  $\Delta T$  is the thermal conductivity temperature difference, and  $\delta$  is the contact surface thickness.  $R_1$  is proportional to  $\delta$  and inversely proportional to  $A$ .

Contact thermal resistance  $R_2$  refers to the additional thermal resistance caused by void air gaps between two surfaces due to the microscopic unevenness of the bonding surfaces of two solids.  $R_2 = \frac{1}{K_t A}$ , where the contact thermal resistance coefficient  $K_t$  is determined by the solid material properties, contact surface roughness, contact pressure, and media type.

In the transient thermal calculation, heat conduction can be realized by assigning a certain thermal resistance in the simulation software. The calculation shows that the internal thermal resistance is 80.8 K/W, and the thermal resistance to the carrier is 2.15 K/W. Higher internal thermal resistance is due to the poor thermal conductivity of the rubber vibration damper. The radiation heat transfer is

$$\Phi_{in2} = \varepsilon_s A_2 \sigma (T_1^4 - T_2^4), \tag{3}$$

where  $\varepsilon_s$  is the system emissivity,  $\sigma$  is the Stefan–Boltzmann constant,  $A_2$  is the radiation surface area,  $T_1$  is the temperature inside the outline cabin, and  $T_2$  is the surface temperature of the optomechanical structure.

**Table 1. Internal Power Consumption of the Camera**

Component	Power Consumption (W)
Plunge angle electric motor	28
Compensated electric motor	28
Parallactic angle electric motor	5.5
Focusing electric motor	2
Temperature control power level	7.5
Power supply component	10
Electric cabinet	40
CCD assembly	15
Sum	136

The internal heat source has significant influence on the temperature distribution of the camera, and its uneven distribution causes the temperature gradient. Table 1 shows the main heat sources inside the camera.

### B. External Thermal Environment

The mounting of the high-altitude vertical imaging aerial camera system on the flight carrier is highly adaptable. The camera is installed on the abdomen of the carrier. The upper part is inside the carrier, while the cylindrical lower part is used as a part of the carrier skin and is directly exposed in the high-altitude environment, as shown in Fig. 1(c). If the flight altitude is 6–20 km, the atmospheric temperature is  $-24$  to  $-55^\circ\text{C}$ , the atmospheric pressure is  $47.2-5.5 \times 10^3$  Pa, and the atmospheric density is  $0.660-0.088$  kg/m<sup>3</sup>, it is a low-temperature, low-pressure, and low-density environment. When the flying height is 6 km, the typical flight Mach number is 0.3 Ma, the flight value is low and belongs to low-speed flight, aerodynamic heat can be ignored, and only the influence of thermal radiation and convective heat transfer on the aviation camera is considered. When the flight altitude is 20 km, the typical flight Mach number is 0.66 Ma, and it is necessary to consider the influence of aerodynamic heating, convection heat transfer, and thermal radiation on the aerial camera.

Considering the actual situation of the constantly changing environment around the camera during flight, there are several heat exchanges between the outside of the camera and the surrounding environment: conduction heat exchange with the carrier  $\Phi_1$ , convective heat exchange with the outside atmosphere  $\Phi_2$ , ground infrared radiation  $\Phi_3$ , solar radiation ground and cloud reflections  $\Phi_4$ , atmospheric radiation  $\Phi_5$ , heat radiated from the outside of the camera  $\Phi_6$ , and aerodynamic heat  $\Phi_7$ .

## 3. THERMAL CONTROL DESIGN

The conventional thermal control method generally implements active and passive thermal control directly on the aerial camera imaging system, and the imaging system cannot be directly isolated from the external environment. The schematic diagram of the principle is shown in Fig. 2(a).

Different from the single layer thermal control method, the multilayer thermal control method divides the aerial camera into the imaging system and the outline cabin without changing the outline size, and uses the material with low thermal conductivity to connect to make the imaging system isolated from the

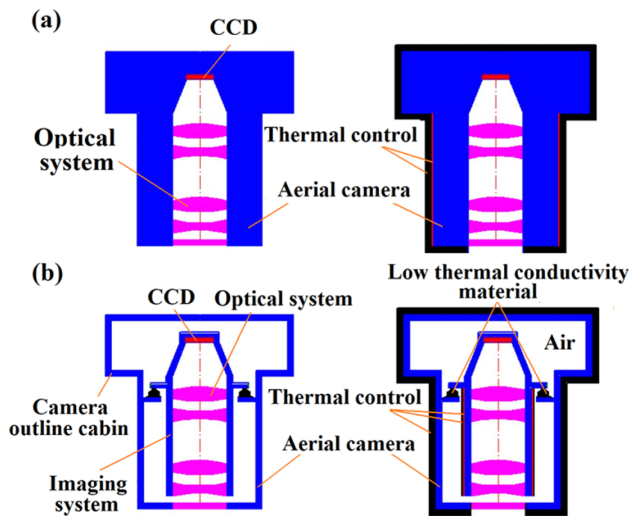


**Fig. 2.** Schematics of (a) single layer and (b) multilayer thermal control principle.

external environment, and then implement active and passive thermal control to form a three-layer thermal control on the outline cabin, air interlayer, and imaging system. The schematic diagram is shown in Fig. 2(b).

For the aerial camera studied in this paper, the first level of thermal control is composed by a thermal insulation layer mounted on the inner surface of the outline cabin for passive thermal control and thermal convection active thermal control on the optical window. The second layer is the air interlayer between the exterior outline cabin and the optical system. It has low thermal conductivity and keeps the inside relatively sealed. The third layer is formed by a heat insulation layer mounted on the outer surface of the optical system and thermal control of the optical element heating film and CCD phase change thermal control.

The overall thermal control guideline is to use the ground air-conditioning insulation device to keep the aerial camera in a constant temperature environment of 20°C. The multilayer thermal control is to maintain the temperature of the optical system to meet the system's thermal control requirements. The whole system mainly includes the defrosting and defogging of the optical window, the temperature maintenance of the optical system lens, and the high-temperature heat dissipation of the CCD, forming a system-level thermal control design combining the passive and active thermal control, as shown in Fig. 3.

### A. Insulation Layer

In order to reduce the heat exchange between the internal optomechanical structure and the external environment, to simultaneously create favorable conditions for active thermal control and to lower the power consumption of active thermal control, the entire interior outline cabin (except for the optical window) and the outside of the imaging system must be covered with a heat insulation layer for thermal insulation.

In order to adapt to the complex environment and through the low-temperature and low-pressure experiment comparison, we selected the microporous polyurethane rubber heat insulation material. The technical specifications are shown in Table 2.

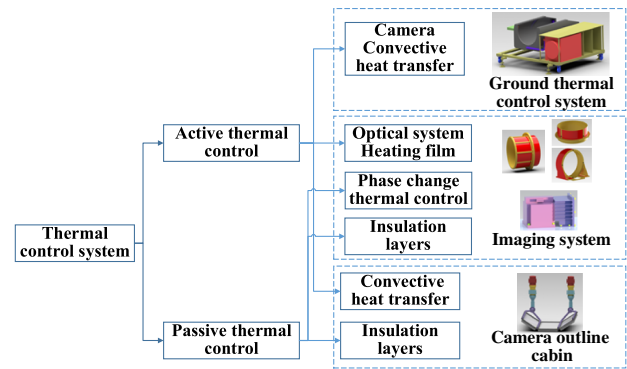


**Fig. 3.** Schematic diagram of ground thermal control and camera system-level thermal control.

**Table 2.** Main Technical Specifications of Microporous Polyurethane Rubber Heat Insulation Materials

Property	Value
Density (kg/m <sup>3</sup> )	240
Thermal conductivity W/(m·°C)	0.086
Coefficient of thermal expansion (m/°C)	5.8–7.8
Standard color	Black
Dimensional stability	±1%
Water absorption, high humidity exposure	2% weight gain
Skin contact irritation	Innocuous

This material has low thermal conductivity, good temperature stability, resistance to low temperature and low pressure, low density, a smooth surface free of impurities, black surface, good flame retardancy, good waterproof and moisture-proof performance, good flexibility, excellent impact absorption ability, good safety, and good operability.

The thickness of microporous polyurethane rubber needs to be determined by the analysis of material thermal resistance and material weight. Material thermal resistance is given by  $R_m = \frac{d}{\lambda_m \cdot A_m}$ , where  $R_m$ ,  $d$ ,  $\lambda_m$ , and  $A_m$  are the thermal resistance, thickness, thermal conductivity, and covering area of the thermal insulation material, respectively. Material thermal resistance is an important parameter to measure the thermal insulation effect of a material, which is proportional to the thickness of the thermal insulation material. The greater the thickness, the higher the thermal resistance, and the better the thermal insulation effect. However, more thickness results in a heavier insulation layer under the same area, which is not suitable for the lightweight design of aviation cameras. In order to ensure the thermal insulation effect and minimize the weight of the thermal insulation layer, the thickness of the thermal insulation material is chosen to be 9.5 mm. The thermal resistance of the thermal insulation layer of the outline cabin is 0.041°C/W, and the weight is 6.16 kg. The thermal resistance of the thermal insulation layer of the imaging system is 0.164°C/W, and the weight is 1.54 kg. Figure 4(a) illustrates the insulation layer of the outline cabin.

### B. Thermal Control of Optical Window

The optical window interfaces the imaging system of the aerial camera and is an important part of the aerial camera imaging. It is directly exposed to the high-altitude, low-temperature, and low-pressure environment during imaging. The external low-temperature environment causes a large temperature difference between the inner and the outer surfaces of the glass window. Frost and fog are formed on the glass surface, block the transmitted light, and seriously affect the imaging quality of the aerial camera.

Considering the structural characteristics of the segmented assembled optical window and the installation space of the convection device, a thermal convection heat exchange device is applied to provide hot air convection on the window glass during the ascent of the flight carrier and during the non-shooting time, as shown in Figs. 4(b) and 4(c). This is to maintain the temperature equilibrium and to avoid the formation of frost and fog on the window. Two sets of fans and heating devices provide hot air to flow through the windpipe, and the air blowing holes are arranged in a staggered arrangement maintaining air circulation on the window. The total power consumption is 40 W.

### C. Thermal Control of Optical System

The optical system is the core of the entire aerial camera. Temperature variation directly affects the image quality of the camera. It requires the most stringent thermal control. After analyzing the thermo-optical characteristics, the lens temperature of the entire optical system requires  $20^{\circ}\text{C} \pm 2.5^{\circ}\text{C}$ . Both axial and radial temperature differences are less than  $5^{\circ}\text{C}$ , respectively.

The polyimide heating film is wrapped on the front lens barrel, focusing lens barrel, rear lens barrel, and other parts where the optical lenses are installed. The partition heating control method is adopted. When the internal and external heat flow conditions change and the temperature of the optical system is affected, active heating compensation is used to maintain the environment temperature. Each heating zone is composed of a heating film, a control unit, and a temperature sensor. The

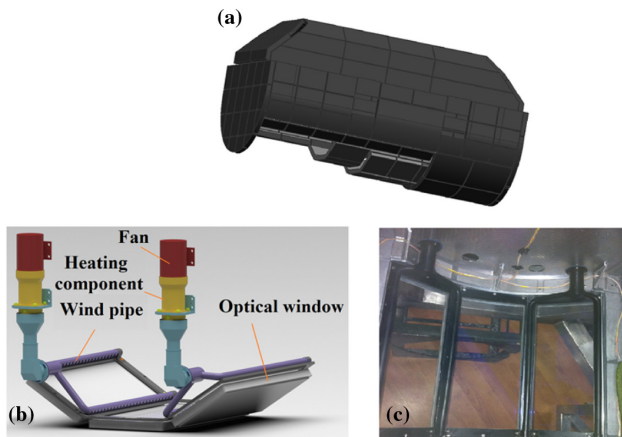


**Fig. 4.** (a) Schematics of the interior of the exterior outline cabin covered with thermal insulation materials, (b) convection thermal control scheme, and (c) physical image of optical window.

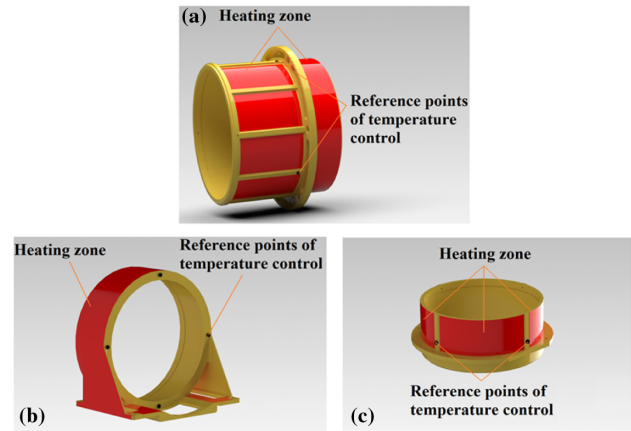


**Fig. 5.** Heating zone of (a) front lens, (b) focusing lens, and (c) rear lens barrel and the position of the temperature control reference point.

heating film and the temperature sensor adopt a dual-circuit cold backup method to improve reliability.

For the lenses, the best temperature control reference point should be placed on the periphery of the lens and arranged evenly. However, due to the limitation of actual operation, the temperature sensor cannot be directly attached on the lenses. The best practical position is evenly arranged on the outer wall of the lens barrel where the lens is mounted. Figure 5(a) shows the heating zone of the front lens barrel and the installation position of the temperature sensor. Two heating zones are arranged symmetrically, and the power consumption of each heating zone is 100 W. Figure 5(b) shows the heating zone of the focusing lens barrel and the installation position of the temperature sensor. The total power consumption is 90 W. Figure 5(c) shows the heating zone of the rear lens barrel and the installation position of the temperature sensor. The total power consumption is 40 W.

### D. CCD Phase Change Thermal Control

The CCD is in continuous working mode. If the heat generated by the CCD cannot be dissipated in time, the temperature of the CCD will rise sharply. It results in rising thermal noise and dark current, and reduces the signal-to-noise ratio of the system and thus the image quality. The actual test shows that after 2 h of continuous operation, the temperature of the CCD rises from  $18^{\circ}\text{C}$  to  $41.4^{\circ}\text{C}$ . The heating rate is too fast, and it exceeds the thermal control requirement of  $18^{\circ}\text{C} - 30^{\circ}\text{C}$ .

Because the CCD is in motion when the camera is working, the traditional heat pipe heat conduction method is not easily implemented. A thermal control method based on phase change n-octadecane material with a fixed melting point is proposed. A completely sealed aluminum alloy packaging container is used to hold the phase change material to prevent liquid phase leakage. The heat dissipation surface of the CCD is filled with thermal grease to absorb the heat from the CCD by thermal conduction and thus cool down the CCD. The schematic diagram is shown in Fig. 6, where the material parameters are shown in Table 3.

Taking  $\Delta T = 10^{\circ}\text{C}$ , where the initial temperature is  $18^{\circ}\text{C}$ , we need 0.0125 kg phase change material. Place the CCD with

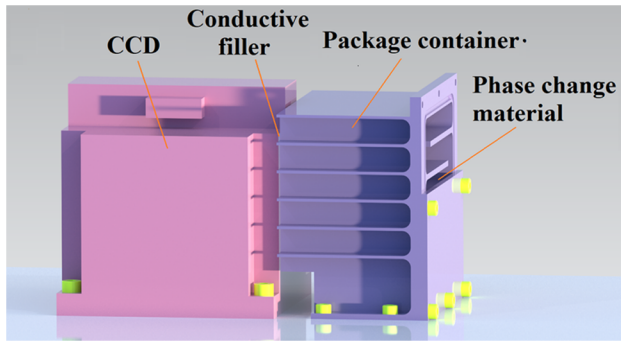


Fig. 6. CCD phase change thermal control composition diagram.

Table 3. Thermophysical Parameters of n-Octadecane

Physical Parameter	Value
Phase transition temperature/°C	28–31
Latent heat J/kg	$2.43 \times 10^5$
Density kg/m <sup>3</sup>	777 (Liquid)
Thermal conductivity W/(m <sup>2</sup> ·°C)	0.1507
Specific heat capacity J/(kg·°C)	$2.16 \times 10^3$

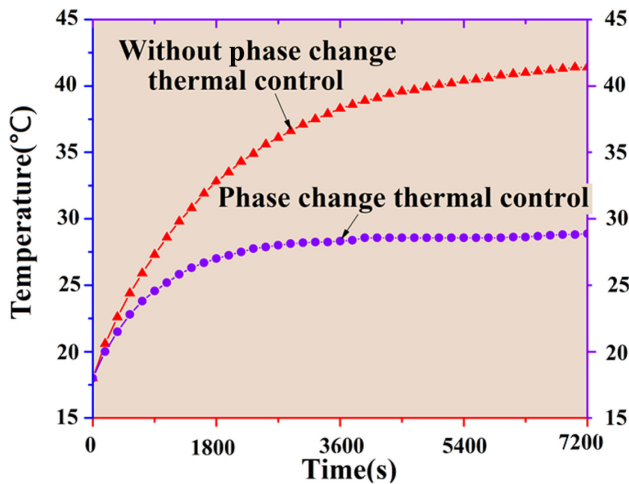


Fig. 7. CCD temperature response curve.

the phase change thermal control device installed in the constant temperature room (18°C), and place four temperature sensors around the CCD; the temperature as a function of time is shown in Fig. 7. After 2 h of continuous operation, the maximum temperature of the CCD without thermal control is 41.4°C, and the heating rate is fast. With thermal control, the maximum temperature of the CCD is 28°C and the heating rate drops significantly. In an indoor environment, the CCD temperature level can be maintained at 18°C–28°C within 2 h.

#### 4. THERMAL SIMULATION ANALYSIS

There are recent approaches for structural–thermal–optical performance analysis and modeling of optical systems [16–18]. Numerical thermal simulation is critical in the entire thermal

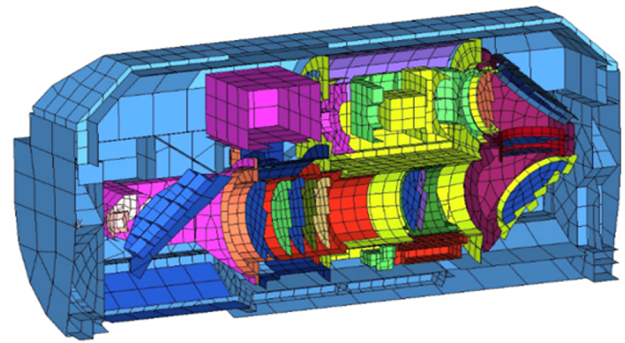


Fig. 8. Thermal analysis model of aerial camera.

control design. It calculates the temperature change of the optical system in the aerial camera based on the internal and external thermal boundary conditions and thermal control measures of the aerial camera. It predicts the actual temperature of the aerial camera under given conditions, and verifies whether the thermal design can control the temperature of the optical system within the required temperature range. The thermal analysis software is used to simplify the thermal model of the aerial camera in accordance with the principle of energy equivalence. The finite element model is shown in Fig. 8. We choose two working conditions. Working condition 1: the initial camera temperature is 20°C, the flying altitude is 20 km, and the flying Mach number is 0.66. Working condition 2: the camera initial temperature is 20°C, the flying height is 6 km, and the flying Mach number is 0.3. Since the first working condition is more demanding, the calculation and analysis of the first working condition are emphasized.

#### A. No Thermal Control Analysis

Figure 9(a) shows the lens temperature cloud picture and the whole machine temperature cloud picture after 2 h under working condition 1 without any thermal control, respectively. The lens temperature is between 4.5 and 15.8°C, the maximum temperature difference is 11.3°C, and the deviation from the initial temperature of 20°C is large. There is a large temperature gradient on the lenses. The imaging system has a large temperature difference.

Figure 9(b) shows the lens temperature cloud picture and the whole machine temperature cloud picture after 2 h under

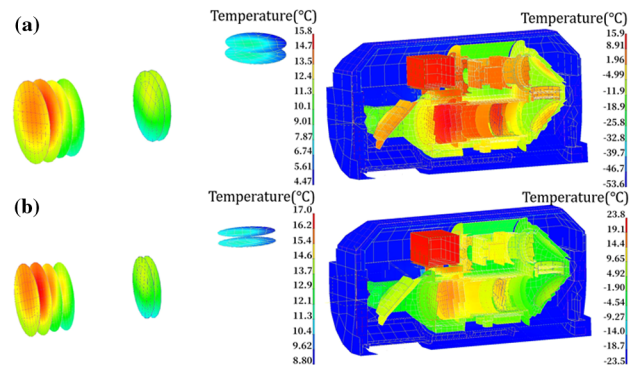
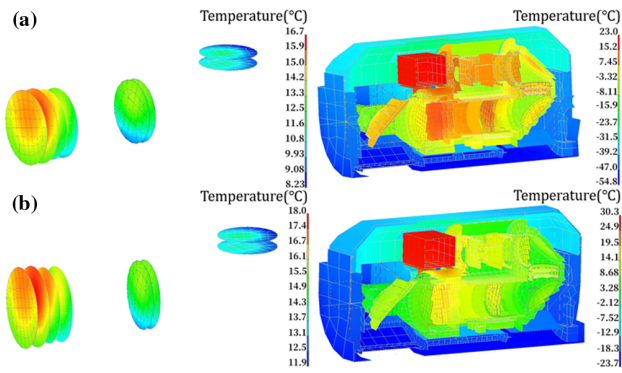


Fig. 9. Lens temperature cloud map and the whole machine temperature cloud map after 2 h without thermal control. (a) Under working condition 1 and (b) under working condition 2.



**Fig. 10.** Lens temperature cloud map and the whole machine temperature cloud map after 2 h with passive thermal control. (a) Under working condition 1 and (b) working condition 2.

working condition 2 without any thermal control. The lens temperature is between 8.8 and 17.0°C, the maximum temperature difference is 8.2°C, and the deviation from the initial temperature is 20°C. There is a large temperature gradient on the lenses. The imaging system has a large temperature difference.

The above results show that the temperature level of the aerial camera will change significantly without thermal control in a low-temperature and low-pressure environment. There is a large temperature gradient between the optical lenses, which cannot meet the thermal control requirements of the optical system. The temperature level of the imaging system decreases as the external temperature decreases.

Figure 10(b) shows the lens temperature cloud picture and the whole machine temperature cloud picture after 2 h under working condition 2 with passive thermal control. The lens temperature is between 11.9 and 18.0°C, and the maximum temperature difference is 6.1°C. The absolute temperature level increases compared to that without thermal control. The outline cabin has a thermal insulation, but the temperature difference of the imaging system is still significant.

The above results show that the temperature level of the aerial camera will increase in a low-temperature and low-pressure environment when passive thermal control measures of the insulation layer are adopted. It indicates that the first and second levels of thermal control are effective. However, a large temperature gradient on the optical lenses cannot meet the thermal control design requirements. In addition, the lower the ambient temperature, the lower the temperature level of the aerial camera.

### B. Overall Thermal Control Analysis

Figure 11(a) shows the lens temperature cloud picture and the whole machine temperature cloud picture after 2 h under working condition 1 with whole thermal control. The lens temperature is between 17.3 and 21.9°C, and the maximum temperature difference is 4.6°C. The deviation from the initial temperature of 20°C is small. The lens temperature gradient is small, and the temperature difference of the imaging system is small.

Figure 11(b) shows the lens temperature cloud picture and the whole machine temperature cloud picture after 2 h under

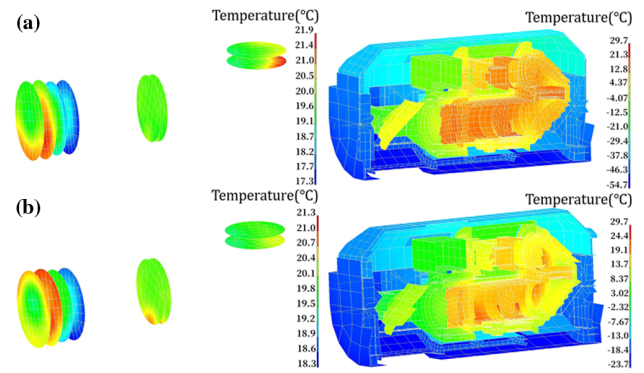


**Fig. 11.** Lens temperature cloud map and the whole machine temperature cloud map after 2 h with whole thermal control. (a) Under working condition 1 and (b) under working condition 2.

working condition 2 with whole thermal control. The lens temperature is between 18.3 and 21.3°C, and the maximum temperature difference is 3.0°C. The deviation from the initial temperature of 20°C is small. The lens temperature gradient is small, and the temperature difference of the imaging system is small.

Therefore, the temperature level of the optical system lens can be maintained at  $20 \pm 2.5^\circ\text{C}$  with the multilayer thermal control method in a low-temperature and low-pressure environment. The temperature difference of the optical and mechanical structure is small, which meets the thermal control requirements of the optical system.

### C. Data Analysis

The external environment temperature ( $-55^\circ\text{C}$ ) of working condition 1 is lower, and the effect of the multilayer thermal control method can be investigated more. Extract the relevant temperature data of working condition 1 for comparison. Figure 12(a) shows the temperature change with time of the lens components inside and outside the exterior outline cabin and the imaging system under working condition 1 without any thermal control. The temperature drop rate of the exterior outline cabin is extremely fast. The temperature drops to

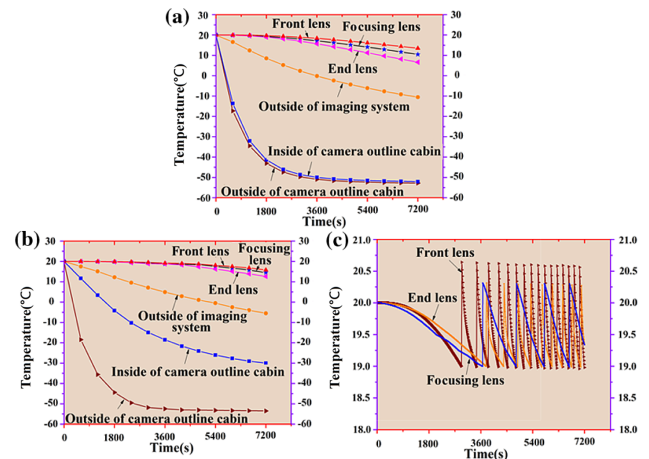


**Fig. 12.** Temperature change curve with time under working condition 1. (a) Without any thermal control, (b) with passive thermal control, and (c) with whole thermal control.

−47.4°C at 2400 s. There is almost no temperature difference between the inside and outside of the outline cabin, and the final temperature is −52.8°C. The outside temperature of the imaging system drops slower. The temperature is 41.5°C higher than the inside temperature of the outline cabin, which is good for maintaining the temperature of the lens components in the imaging system. All lenses maintain a good temperature level within 2400 s ( $20^{\circ}\text{C} \pm 2.5^{\circ}\text{C}$ ). The lowest temperature is 18.1°C. But the temperature level of all lenses has a speeding decrease along the time, and the temperature difference between lenses becomes larger.

Figure 12(b) shows the temperature change with time of the lens components inside and outside the exterior outline cabin and the imaging system under working condition 1 with passive thermal control. With passive thermal control, the temperature drop rate inside the outline cabin is significantly slower. At 7200 s, the lowest temperature is  $-30^{\circ}\text{C}$ , indicating that the outline cabin has a good thermal insulation effect. The temperature level outside the imaging system increases  $5.5^{\circ}\text{C}$  at maximum over that without any thermal control measures. All lenses maintain a better temperature level ( $20^{\circ}\text{C} \pm 2.5^{\circ}\text{C}$ ) within 4200 s, and the lowest temperature is  $18.3^{\circ}\text{C}$ . The overall temperature level of the lenses declines along the time, but the rate slows down. The lowest temperature increases by a maximum of  $6^{\circ}\text{C}$  compared to that without thermal control.

Figure 12(c) shows the temperature change with time of the temperature control point of the lens assembly with the whole thermal control under working condition 1. The temperature overshoot value of the temperature control point of the lens assembly is within  $1.5^{\circ}\text{C}$ , and the temperature uniformity is good, which meets the thermal control requirements.

Comparing the above data, we can obtain the following conclusions:

1. After the first and second layers of thermal control are implemented, the maximum temperature difference between the lenses is reduced from  $11.3^{\circ}\text{C}$  to  $8.5^{\circ}\text{C}$ . The first and second layers of thermal control increase the temperature level of the optical lenses and reduce the temperature gradient. They increase the thermal inertia of the aerial camera, prolong the retention time of the temperature level, reduce the influence of the external environment on the camera imaging system, slow down the overall cooling speed, and improve the temperature uniformity.
2. After multilayer thermal control is implemented, the maximum temperature difference between the lenses is reduced from  $11.3^{\circ}\text{C}$  to  $4.6^{\circ}\text{C}$ , which meets the thermal control requirement. The multilayer thermal control greatly increases the temperature level of the camera and effectively controls the temperature gradient of the optical system.
3. The temperature level of the external environment has a greater impact on the internal temperature distribution of the aerial camera. The lower the external environment temperature, the lower the overall temperature level of the camera, and the greater the difficulty of thermal control. It provides a favorable theoretical basis for the thermal test. The thermal test is carried out according to working condition 1.

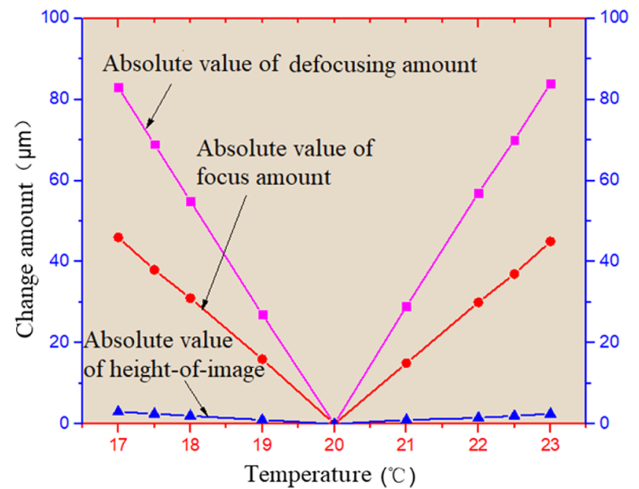


Fig. 13. Results of thermal optical analysis.

#### D. Thermal Optical Analysis

The main factors affecting the thermal optical properties are the refractive index of the lens optical material and the linear expansion coefficient of the lens material and lens barrel material. The lens materials are ZBAF1, ZBAF3, and TF3, and the lens barrel material is TC4. Through temperature analysis of the optical system, the influence of temperature change on the defocusing amount, focus, and height-of-image of the optical system is obtained as shown in Fig. 13.

When the lens temperature varies from  $17.3^{\circ}\text{C}$  to  $21.9^{\circ}\text{C}$ , the maximum absolute value of focus amount of the optical system is  $39\ \mu\text{m}$ , which is acceptable.

### 5. THERMAL EQUILIBRIUM TEST AND FLIGHT TEST

#### A. Thermal Equilibrium Test

The thermal equilibrium test of the aerial camera is relatively complicated and difficult. The laws and methods of various thermal tests need to be continuously explored during the test process. With existing laboratory conditions, it is impossible to simulate the external boundary conditions such as wind tunnels (convection heat transfer), but the low-temperature and low-pressure environment can be used to verify the effect of active thermal control. The thermal equilibrium test equipment of the camera is shown in Fig. 14, which is mainly composed of environmental equipment and testing equipment.

Figure 15(a) shows the temperature change with time of the temperature control point of all lenses. The temperature overshoot value of the temperature control point of the lenses is within  $1^{\circ}\text{C}$ . The experiment result is better than the simulation result. This is because the simulation step is 10 s in the thermal analysis. In the experiment, the control period is 1 s, and the thermal control accuracy is higher.

Figure 15(b) shows the CCD temperature change curve with time. Within 2 h of continuous operation, the CCD's temperature rises slowly and the maximum temperature is  $29.4^{\circ}\text{C}$ , which is slightly higher than the laboratory environment temperature and meets the thermal control requirements.

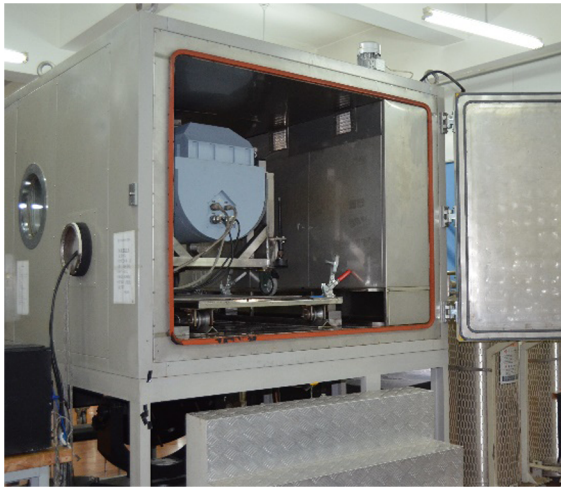


Fig. 14. Actual thermal test equipment.



Fig. 16. Aerial image.

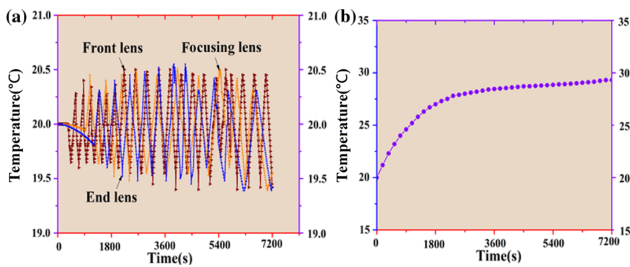


Fig. 15. (a) Time dependent temperature curve of the temperature control point of the lenses in the thermal test and (b) CCD temperature change curve with time.

**B. Flight Test**

Flight test is the most direct and effective way to check the thermal control effect of the aerial camera. It can avoid errors caused by simulated calculation of thermal boundary conditions and thermal coupling, and can truly reflect the temperature distribution and imaging results of high-altitude aerial cameras. We use actual installation condition on the aircraft, the flying altitude is about 6 km, and the flying Mach number is about 0.3 Ma. During the flight test, no frosting or fogging was observed on the optical window, the CCD worked normally, and high-quality aerial images were obtained, as shown in Fig. 16.

The temperature distribution of various parts of the aerial camera after 2 h is shown in Table 4. The temperature distribution of the aerial camera measured during the flight is basically the same as the thermal calculation result, with a maximum error of 6.7%, which is caused by various errors such as low-temperature simulation error, external heat flow simulation error, and thermal coupling error. Moreover, the temperature difference of the interior and exterior outline cabin and the surface temperature of the imaging system have little impact on the imaging quality of the aerial camera. Therefore, the maximum error of 6.7% is acceptable. For the lens group, since the active thermal control period in the actual flight test is 1 s, and the calculation step length in the thermal analysis is 10 s, the actual flight test results are better than the analysis results.

**Table 4. Actual Flight and Thermal Simulation Analysis Temperature Control Point Data of the Aerial Camera after 2 h**

Point for Measuring Temperature	Initial Temperature (°C)	Actual Temperature (°C)	Simulation Temperature (°C)
Exterior surface of camera	19.7	-22.2	-23.7
Inside of camera outline cabin	19.8	-12.1	-13.0
Outside of optic-mechanical structure	19.8	9.0	8.4
Front lens component	19.9	20.1	20.7
Focusing lens component	19.9	19.9	20.5
End lens component	19.9	19.8	20.6

Given the thermal test results and the flight images, the multilayer thermal control method can effectively increase the overall temperature level of the imaging system, and effectively control the temperature level and temperature gradient of the optical lenses, which contribute to acquiring stable and clear aerial images.

**6. CONCLUSION**

The single layer thermal control method is known to increase the thermal control power consumption and the difficulty of thermal control. We propose a multilayer and system-level thermal control system for aerial cameras, especially for those are directly exposed to the external environment during work. Based on detailed analysis of the internal and external thermal environment of the high-altitude vertical imaging aerial cameras, the effective thermal isolation of the optical system from the complex external environment is achieved by using a rubber damper, a thermal insulation outline cabin, and an internal air interlayer. The lens temperature in the optical system is well buffered, and the active thermal control power consumption is

effectively reduced. This distinguishes our method from the traditional thermal control method. In addition, the system-level thermal control design is provided from the optical window, the optical system lens to CCD, so as to obtain higher-quality aerial images. Thermal simulation analysis and thermal test results show that the thermal control power consumption of the system is 270 W, the temperature gradient of the optical system does not exceed 5°C, and the CCD temperature does not exceed 30°C, which meets the thermal control design requirements. Therefore, the multilayer thermal control method is simple, accurate, low-cost, easy to implement, and can effectively reduce thermal control power consumption and the difficulty of thermal control. This method has been successfully applied to high-altitude vertical imaging aerial cameras, and high-quality aerial images have been obtained. In this paper, the exterior outline cabin is sealed but not airtight. In the future, airtight outline cabins can be studied to further improve the thermal insulation effect.

**Funding.** National Natural Science Foundation of China (61405192).

**Disclosures.** The authors declare no conflicts of interest.

**Data availability.** Data underlying the results presented in this paper are not publicly available at this time but may be obtained from the authors upon reasonable request.

## REFERENCES

1. S. G. Loegering, "The global hawk/BAMS navigation system; an update to the odyssey," *J. Navig.* **64**, 15–27 (2011).
2. K. J. Held and B. H. Robinson, "TIER II Plus airborne EO sensor LOS control and image geolocation," *Proc. IEEE* **2**, 377–405 (1997).
3. A. G. Lareau, A. J. Partynski, and W. G. Fishell, "Dual-band framing cameras: technology and status," *Proc. SPIE* **4127**, 148–156 (2000).
4. M. Iyengar and D. Lange, "The Goodrich 3(rd) generation DB-110 system: operational on tactical and unmanned aircraft," *Proc. SPIE* **6209**, 620909 (2006).
5. S. Koeber, R. Palmer, M. Laueremann, W. Heni, D. L. Elder, D. Korn, M. Woessner, L. Alloatti, S. Koenig, and P. C. Schindler, "Femtojoule electro-optic modulation using a silicon-organic hybrid device," *Light Sci. Appl.* **4**, e255 (2015).
6. W. G. Yang, L. Yu, R. L. Chen, and Y. C. Li, "Precise thermal control design and validation for high resolution space camera," *Acta Photon. Sin.* **38**, 2363–2367 (2009) (in Chinese).
7. E. Jakel, W. Erne, and G. Soulat, "The thermal control system of the Faint Object Camera /FOC," in *15th Thermophysics Conference* (2010), p. 1501.
8. I. Colomina and P. Molina, "Unmanned aerial systems for photogrammetry and remote sensing: a review," *ISPRS J. Photogr. Remote Sens.* **92**, 79–97 (2014).
9. F. Liu, Z. Cheng, P. Jia, B. Zhang, and R. Hu, "Impact of thermal control measures on the imaging quality of an aerial optoelectronic sensor," *Sensors* **19**, 2753 (2019).
10. W. Liu, H. Shen, Y. Xu, Y. Song, H. Li, J. Jia, and Y. Ding, "Developing a thermal control strategy with the method of integrated analysis and experimental verification," *Optik* **126**, 2378–2382 (2015).
11. Y. Fan, W. Liang, and W. Mang, "Thermal design of the optical system in an aerial camera," *Opto Electron. Eng.* **40**, 51–59 (2013).
12. W. Y. Liu, Y. L. Ding, Q. W. Wu, J. Q. Jia, G. Liang, and L. H. Wang, "Thermal analysis and design of the aerial camera's primary optical system components," *Appl. Therm. Eng.* **38**, 40–47 (2012).
13. Z. Cheng, L. Sun, F. Liu, X. Liu, L. Li, Q. Li, and R. Hu, "Engineering design of an active-passive combined thermal control technology for an aerial optoelectronic platform," *Sensors* **19**, 5241 (2019).
14. M. Bahrami, M. M. Yovanovich, and J. R. Culham, "Thermal contact resistance at low contact pressure: effect of elastic deformation," *Int. J. Heat Mass Transfer* **48**, 3284–3293 (2005).
15. Y. G. Lee, D. M. Kim, and C. H. Yeom, "Development of Korean high altitude platform systems," *Int. J. Wirel. Inf. Netw.* **13**, 31–42 (2006).
16. A. Haber, J. E. Draganov, K. Heesh, J. Tesch, and M. Krainak, "Modeling and system identification of transient STOP models of optical systems," *Opt. Express* **28**, 39250–39265 (2020).
17. A. Haber, J. E. Draganov, K. Heesh, J. Cadena, and M. Krainak, "Modeling, experimental validation, and model order reduction of mirror thermal dynamics," *Opt. Express* **29**, 24508–24524 (2021).
18. C. Lyu and R. Zhan, "STOP model development and analysis of an optical collimation system for a tactical high-energy laser weapon," *Appl. Opt.* **60**, 3596–3603 (2021).